ADER SCHEMES FOR THREE-DIMENSIONAL NONLINEAR HYPERBOLIC SYSTEMS

V.A. Titarev[1] and E.F. Toro[2]

[1] Department of Mathematics, Faculty of Science,
University of Trento, Trento, Italy,
E-mail: titarev@science.unitn.it,
Web page: http://www.science.unitn.it/∼titarev

[2] Laboratory of Applied Mathematics, Faculty of Engineering,
University of Trento, Trento, Italy,
E-mail: toro@ing.unitn.it,
Web page: http://www.ing.unitn.it/toro

In this paper we carry out the extension of the ADER approach to multidimensional non-linear systems of conservation laws. We implement non-linear schemes of up to fourth order of accuracy in *both time and space*. Numerical results for the compressible Euler equations illustrate the very high order of accuracy and non-oscillatory properties of the new schemes. Compared to the state-of-art finite-volume WENO schemes the ADER schemes are faster, more accurate and need less computer memory.

1 Introduction

The class of Godunov-type methods for solving numerically hyperbolic conservation laws is often regarded as one of the most successful. The original first-order scheme of Godunov [5, 6, 7] uses the self-similar solution of the local Riemann problem with piece-wise constant initial data to compute the upwind numerical flux. The extension to second order of accuracy in time and space can be carried out, amongst other ways, by using a non-oscillatory piece-wise linear reconstruction of data from cell averages [12, 13, 39] and solving the generalised Riemann problem at cell interface position. The generalisation of the Riemann problem here consists of using the initial condition in the form of two linear reconstruction polynomials instead of the piece-wise constant states, as done in the first-order scheme. The corresponding Generalised Riemann Problem (GRP) schemes in one space dimension have been constructed by various authors [2, 14, 16].

In general, the approximate solution of the generalised Riemann problem, given in [15] for one-dimensional Euler equations of a gamma-law gas, is quite cumbersome and may be not possible to obtain for more complicated hyperbolic systems, e.g. MHD equations. Therefore, the GRP-type methods as such are not competitive with other second-order accurate Godunov methods. A major simplification to the GRP methodology comes with the modified GRP (MGRP) scheme, proposed in [28]. In this scheme the generalised Riemann problem is not solved directly. Instead, it is replaced by two conventional Riemann problems, namely one non-linear problem for the leading term for state variables and one linear problem for gradients of state variables. Since approximate-state Riemann solvers are available for most of the hyperbolic conservation laws of interest, the MGRP scheme is much more practical than the original GRP schemes [2, 14, 16].

The ADER approach [30, 31] can be regarded as a further development of the MGRP scheme in that it breaks the barrier of second-order accuracy and allows the construction of *arbitrarily* high-order accurate schemes, both in time and space. To evaluate the numerical flux, in the ADER approach one solves the generalised Riemann problem with initial condition consisting of two arbitrary but smooth functions using a semi-analytical method, reported in [32]. The approximate solution is given as a Taylor time expansion at the cell interface position up to any order of time accuracy $1 \leq r < \infty$. The extension of original ADER schemes [31] to the one-dimensional nonlinear systems, using the method [32] has been reported in [26, 33]. See also [25, 27]. In multiple space dimensions the nonlinear ADER schemes as applied to scalar nonlinear equations have been constructed in [34, 11] for both structured and unstructured meshes. We also mention [20, 21] where the authors consider *linear* (fixed-stencil) ADER schemes for two-dimensional linear homogeneous systems with constant coefficients systems. So far the approach has not been applicable to multidimensional nonlinear systems.

The motivation of this paper is to carry out the extension of one-dimensional non-oscillatory ADER schemes [26] to multidimensional nonlinear systems of conservation laws. We present numerical results of schemes of third and fourth order of time accuracy as applied to the compressible Euler equations of gas dynamics in two and three space dimensions. These results illustrate the very high order of accuracy of the schemes as well as their essentially non-oscillatory behaviour. When compared with the state-of-art finite-volume WENO scheme of Shi *et. al* [22], the ADER schemes are faster, more accurate and need less computer memory.

The rest of the paper is organized as follows. In Section 2 we very briefly review the ADER approach as applied to one-dimensional nonlinear systems. Extension to three-dimensional nonlinear systems is carried out in Section 3. Numerical results are provided in Section 4 and conclusions are drawn in Section 5.

2   The numerical scheme in one space dimension

Consider a hyperbolic system in conservation form given by

$$\partial_t \mathbf{Q} + \partial_x \mathbf{F}(\mathbf{Q}) = \mathbf{0} \qquad (1)$$

along with initial and boundary conditions. Here $\mathbf{Q}$ is the vector of unknown conservative variables and $\mathbf{F}(\mathbf{Q})$ is the physical flux vector. Integrating (1) over a space-time control volume in $x - t$ space $[x_{i-1/2}, x_{i+1/2}] \times [t^n, t^{n+1}]$ of dimensions $\Delta x = x_{i+1/2} - x_{i-1/2}$, $\Delta t = t^{n+1} - t^n$, we obtain the following one-step finite-volume scheme:

$$\mathbf{Q}_i^{n+1} = \mathbf{Q}_i^n + \frac{\Delta t}{\Delta x} \left(\mathbf{F}_{i-1/2} - \mathbf{F}_{i+1/2} \right). \qquad (2)$$

Here $\mathbf{Q}_i^n$ is the cell average of the solution at time level t^n, $\mathbf{F}_{i+1/2}$ is the time average of the physical flux at cell interface $x_{i+1/2}$:

$$\mathbf{Q}_i^n = \frac{1}{\Delta x} \int_{x_{i-1/2}}^{x_{i+1/2}} \mathbf{Q}(x, t^n) \, dx, \quad \mathbf{F}_{i+1/2} = \int_{t^n}^{t^{n+1}} \mathbf{F}(\mathbf{Q}(x_{i+1/2}, t)) \, dt. \qquad (3)$$

The first step in the ADER flux evaluation algorithm is the reconstruction of point-wise values of the solution from cell averages at $t = t^n$ via high-order polynomials. To circumvent the Godunov theorem [5] and design non-oscillatory schemes we use the non-linear (solution-adaptive) weighted essentially non-oscillatory (WENO) reconstruction, see [10, 1, 22] and references therein. We remark that for the rth order accurate scheme (in time and space) the reconstruction polynomials must be of $(r - 1)^{\text{th}}$ order, e.g. for third order schemes we use piece-wise parabolic reconstruction and so on.

After the reconstruction step the conservative variables in each cell are represented by vectors $\mathbf{p_i}(x)$ of polynomials. Then at each cell interface we can pose the following generalised Riemann problem:

$$
\begin{aligned}
\text{PDE:} &\quad \partial_t \mathbf{Q} + \partial_x \mathbf{F}(\mathbf{Q}) = \mathbf{0}, \\
\text{IC:} &\quad \mathbf{Q}(x, 0) = \begin{cases} \mathbf{Q}_L(x) = \mathbf{p}_i(x), & x < x_{i+1/2}, \\ \mathbf{Q}_R(x) = \mathbf{p}_{i+1}(x), & x > x_{i+1/2}. \end{cases}
\end{aligned} \qquad (4)
$$

We find an approximate solution for the interface state $\mathbf{Q}(x_{i+1/2}, \tau)$, where τ is local time $\tau = t - t^n$, using a semi-analytical method developed in [32]. For r^{th} order of accuracy the method reduces the difficulty of solving the generalised Riemann problem (4) to that of solving a sequence of conventional Riemann problems, namely one nonlinear and $(r - 1)$ linear problems, and proceeds as follows. First we write a Taylor expansion of the interface state in time

$$\mathbf{Q}(x_{i+1/2}, \tau) = \mathbf{Q}(x_{i+1/2}, 0+) + \sum_{k=1}^{r-1} \left[\frac{\partial^k}{\partial t^k} \mathbf{Q}(x, t)(x_{i+1/2}, 0+) \right] \frac{\tau^k}{k!}. \qquad (5)$$

3

The leading term $\mathbf{Q}(x_{i+1/2}, 0+)$ accounts for the first-instant interaction of the boundary extrapolated values $\mathbf{Q}_L(x_{i+1/2})$ and $\mathbf{Q}_R(x_{i+1/2})$ and is the Godunov state [5] of the conventional (piece-wise constant data) Riemann problem:

$$\partial_t \mathbf{Q} + \partial_x \mathbf{F}(\mathbf{Q}) = \mathbf{0},$$

$$\mathbf{Q}(x, 0) = \begin{cases} \mathbf{Q}_L(x_{i+1/2}) & \text{if} \quad x < x_{i+1/2}, \\ \mathbf{Q}_R(x_{i+1/2}) & \text{if} \quad x > x_{i+1/2}. \end{cases} \tag{6}$$

A key ingredient here is the availability of an exact or approximate Riemann solver to provide this first term in the expansion.

The higher order terms are evaluated in two steps. First we express all time derivatives via spatial derivatives by means of the Cauchy-Kowalewski procedure. For system (1) the procedure yields the following expressions:

$$\partial_t \mathbf{Q} = -\left(\frac{\partial \mathbf{F}}{\partial \mathbf{Q}}\right) \partial_x \mathbf{Q},$$

$$\partial_{tx} \mathbf{Q} = -\left(\frac{\partial^2 \mathbf{F}}{\partial \mathbf{Q}^2}\right) (\partial_x \mathbf{Q})^2 - \left(\frac{\partial \mathbf{F}}{\partial \mathbf{Q}}\right) \partial_{xx} \mathbf{Q}, \tag{7}$$

$$\partial_{tt} \mathbf{Q} = -\left(\frac{\partial^2 \mathbf{F}}{\partial \mathbf{Q}^2}\right) \partial_t \mathbf{Q} \partial_x \mathbf{Q} - \left(\frac{\partial \mathbf{F}}{\partial \mathbf{Q}}\right) \partial_{xt} \mathbf{Q}$$

and so on. In practice, we find it more convenient to carry out (7) in componentwise manner rather than in the matrix form. The procedure can be easily coded with the aid of algebraic manipulators, such as MAPLE or Mathematica.

Next we derive the evolution equations for the spatial derivatives by differentiating the governing equation (1) and reconstruction polynomials $\mathbf{Q}_L$, $\mathbf{Q}_R$ with respect to x. In general, for nonlinear systems the evolution equation for each spatial derivative

$$\mathbf{Q}^{(k)} \equiv \frac{\partial^k}{\partial x^k} \mathbf{Q}, \quad 1 \le k \le r - 1$$

is in non-conservative form and contains a nonlinear source term $\mathbf{H}$ depending on derivatives of lower order $l = 1, \ldots k - 1$ as well as $\mathbf{Q}(x, t)$ itself:

$$\partial_t \left(\mathbf{Q}^{(k)}\right) + \mathbf{A} \partial_x \left(\mathbf{Q}^{(k)}\right) = \mathbf{H}(\mathbf{Q}, \mathbf{Q}^{(1)}, \mathbf{Q}^{(2)}, \ldots \mathbf{Q}^{(k-1)}), \quad k = 1, \ldots r - 1. \tag{8}$$

For the Taylor expansion (5) we need the solution of (8) for each $k = 1, \ldots r - 1$ at interface position $x = x_{i+1/2}$ at time $\tau = 0+$. Therefore, we can neglect the influence of the source term, which comes into effect for $\tau > 0$ only. Additionally, we linearize the equation around the leading term $\mathbf{Q}(x_{i+1/2}, 0+)$ of the time expansion (5) and replace the piece-wise polynomial initial data by left and right boundary extrapolated values of spatial derivatives at $x_{i+1/2}$. The described simplifications result in the following linear conventional Riemann problem for the spatial derivatives $\mathbf{Q}^{(k)}$:

$$\partial_t \left(\mathbf{Q}^{(k)}\right) + \mathbf{A}_{i+1/2} \partial_x \left(\mathbf{Q}^{(k)}\right) = \mathbf{0}, \quad \mathbf{A}_{i+1/2} = \mathbf{A}(\mathbf{Q}(x_{i+1/2}, 0+)),$$

$$\mathbf{Q}^{(k)}(x, 0) = \begin{cases} \dfrac{\partial^k}{\partial x^k} \mathbf{Q}_L(x_{i+1/2}), & x < x_{i+1/2}, \\ \dfrac{\partial^k}{\partial x^k} \mathbf{Q}_R(x_{i+1/2}), & x > x_{i+1/2}. \end{cases} \tag{9}$$

4

Note that the coefficient matrix $\mathbf{A}_{i+1/2}$ is the same for all derivatives and has to be evaluated only once. If we denote by $\mathbf{Q}_*^{(k)}((x - x_{i+1/2})/\tau)$ the self-similar solution of (9), then the spatial derivatives $\mathbf{Q}^{(k)}$ in (9) are computed as $\mathbf{Q}^{(k)} = \mathbf{Q}_*^{(k)}(0)$, the Godunov state.

Finally, having found all spatial derivatives we form the Taylor expansion (5). Two options now exist to evaluate the numerical flux. The first option is the *state-expansion* ADER [26], in which the approximate state (5) is inserted into the definition of the numerical flux (3) and then an appropriate r^{th}-order accurate quadrature is used for time integration:

$$\mathbf{F}_{i+1/2} = \sum_{l=0}^{K_l} \mathbf{F}(\mathbf{Q}(x_{i+1/2}, \gamma_l \Delta t))\omega_l. \tag{10}$$

Here γ_j and ω_j are properly scaled nodes and weights of the rule and K_α is the number of nodes.

The second option to evaluate the numerical flux is the *flux-expansion* ADER [33, 25], in which we seek Taylor time expansion of the physical flux at $x_{i+1/2}$:

$$\mathbf{F}(x_{i+1/2}, \tau) = \mathbf{F}(x_{i+1/2}, 0+) + \sum_{k=1}^{r-1} \left[\frac{\partial^k}{\partial t^k} \mathbf{F}(x_{i+1/2}, 0+) \right] \frac{\tau^k}{k!}. \tag{11}$$

From (3) and (12) the numerical flux is now given by

$$\mathbf{F}_{i+1/2} = \mathbf{F}(x_{i+1/2}, 0+) + \sum_{k=1}^{r-1} \left[\frac{\partial^k}{\partial t^k} \mathbf{F}(x_{i+1/2}, 0+) \right] \frac{\Delta t^k}{(k+1)!}. \tag{12}$$

The leading term $\mathbf{F}(x_{i+1/2}, 0+)$ accounts for the first interaction of left and right boundary extrapolated values and is computed as a certain monotone flux of the conventional Riemann problem (6) for the leading term of the state expansion (5). Following [33], the remaining higher order time derivatives of the flux in (12) are expressed via time derivatives of the intercell state $\mathbf{Q}(x_{i+1/2}, 0+)$, which are known from (5). No numerical quadrature is then required to compute the numerical flux.

The solution is advanced in time by updating the cell averages according to the one-step formula (2).

3 Extension to several space dimensions

Consider the following three-dimensional nonlinear system of conservation laws:

$$\partial_t \mathbf{Q} + \partial_x \mathbf{F}(\mathbf{Q}) + \partial_y \mathbf{G}(\mathbf{Q}) + \partial_z \mathbf{H}(\mathbf{Q}) = \mathbf{0}. \tag{13}$$

Integration of (13) over a space-time control volume of dimensions $\Delta x = x_{i+1/2} - x_{i-1/2}$, $\Delta y = y_{j+1/2} - y_{j-1/2}$, $\Delta z = z_{k+1/2} - z_{k-1/2}$, $\Delta t = t^{n+1} - t^n$ produces the following one-step finite-volume scheme:

$$\begin{aligned} \mathbf{Q}_{ijk}^{n+1} = \mathbf{Q}_{ijk}^n \quad &+ \frac{\Delta t}{\Delta x} \left(\mathbf{F}_{i-1/2,jk} - \mathbf{F}_{i+1/2,jk} \right) + \frac{\Delta t}{\Delta y} \left(\mathbf{G}_{i,j-1/2,k} - \mathbf{G}_{i,j+1/2,k} \right) \\ &+ \frac{\Delta t}{\Delta z} \left(\mathbf{H}_{ij,k-1/2} - \mathbf{H}_{ij,k+1/2} \right), \end{aligned} \tag{14}$$

where $\mathbf{Q}_{ijk}^n$ is the cell average of the solution at time level t^n:

$$\mathbf{Q}_{ijk}^n = \frac{1}{\Delta x}\frac{1}{\Delta y}\frac{1}{\Delta z} \int_{x_{i-1/2}}^{x_{i+1/2}} \int_{y_{j-1/2}}^{y_{j+1/2}} \int_{y_{j-1/2}}^{y_{j+1/2}} \mathbf{Q}(x,y,z,t^n)\,dz\,dy\,dx, \qquad (15)$$

and $\mathbf{F}_{i+1/2,jk}$, $\mathbf{G}_{i,j+1/2,k}$ and $\mathbf{H}_{ij,k+1/2}$ are the space-time averages of the physical fluxes at the cell interfaces:

$$\mathbf{F}_{i+1/2,jk} = \frac{1}{\Delta t}\frac{1}{\Delta y}\frac{1}{\Delta z} \int_{y_{j-1/2}}^{y_{j+1/2}} \int_{z_{k-1/2}}^{z_{k+1/2}} \int_{t^n}^{t^{n+1}} \mathbf{F}(\mathbf{Q}(x_{i+1/2},y,z,\tau))\,d\tau\,dz\,dy,$$

$$\mathbf{G}_{i,j+1/2,k} = \frac{1}{\Delta t}\frac{1}{\Delta x}\frac{1}{\Delta z} \int_{x_{i-1/2}}^{x_{i+1/2}} \int_{z_{k-1/2}}^{z_{k+1/2}} \int_{t^n}^{t^{n+1}} \mathbf{G}(\mathbf{Q}(x,y_{i+1/2},z,\tau))\,d\tau\,dz\,dx, \qquad (16)$$

$$\mathbf{H}_{ij,k+1/2} = \frac{1}{\Delta t}\frac{1}{\Delta x}\frac{1}{\Delta y} \int_{x_{i-1/2}}^{x_{i+1/2}} \int_{y_{j-1/2}}^{y_{j+1/2}} \int_{t^n}^{t^{n+1}} \mathbf{H}(\mathbf{Q}(x,y,z_{i+1/2},\tau))\,d\tau\,dy\,dx.$$

Here $\tau = t - t^n$ is local time.

While describing the procedure to evaluate the numerical flux in three space dimensions we concentrate on $\mathbf{F}_{i+1/2,jk}$; the expressions for $\mathbf{G}_{i,j+1/2,k}$ and $\mathbf{H}_{ij,k+1/2}$ are obtained in an entirely analogous manner.

The evaluation of the ADER numerical flux $\mathbf{F}_{i+1/2,jk}$ consists of the following steps. First we discretize the spatial integrals over the cell faces in (16) using a tensor product of a suitable Gaussian numerical quadrature. The expression for the numerical flux in the x coordinate direction then reads

$$\mathbf{F}_{i+1/2,jk} = \sum_{\alpha=1}^{N} \sum_{\beta=1}^{N} \left(\frac{1}{\Delta t} \int_{t^n}^{t^{n+1}} \mathbf{F}(\mathbf{Q}(x_{i+1/2},y_\alpha,z_\beta,\tau))d\tau \right) K_\beta\,K_\alpha, \qquad (17)$$

where y_α, z_β are the integration points over the cell face $[x_{i-1/2},x_{i+1/2}]\times[y_{j-1/2},y_{j+1/2}]$ and K_α, K_β are the weights. Normally, we use the two-point Gaussian quadrature for third and fourth order schemes and a higher-order Gaussian quadrature for fifth and higher order schemes.

Next we reconstruct the point-wise values of the solution and all derivatives up to order $r-1$ from cell averages at the Gaussian integration points $(x_{i+1/2},y_\alpha,z_\beta)$ by means of the dimension-by-dimension WENO reconstruction. For general information on reconstruction in the context of the two-dimensional ENO and WENO schemes see [3, 22]. Extension to three space dimensions in the context of ADER schemes can be found in [34].

After the reconstruction is carried out for each Gaussian integration point (y_α,z_β) at the cell face we pose the generalised Riemann problem (4) in the x-coordinate direction (normal to the cell boundary) and obtain a high order approximation to $\mathbf{Q}(x_{i+1/2},y_\alpha,z_\beta,\tau)$. All steps of the solution procedure remain *essentially* as in the one-dimensional case. We write Taylor series expansion in time

$$\mathbf{Q}(x_{i+1/2},y_\alpha,z_\beta,\tau) = \mathbf{Q}(x_{i+1/2},y_\alpha,z_\beta,0+) + \sum_{k=1}^{r-1} \left[\frac{\partial^k}{\partial t^k}\mathbf{Q}(x_{i+1/2},y_\alpha,z_\beta,0+) \right] \frac{\tau^k}{k!}. \qquad (18)$$

The leading term $\mathbf{Q}(x_{i+1/2}, y_\alpha, z_\beta, 0+)$ is the Godunov state of the conventional Riemann problem

$$
\left.
\begin{array}{l}
\partial_t \mathbf{Q} + \partial_x \mathbf{F}(\mathbf{Q}) = \mathbf{0}, \\[2mm]
\mathbf{Q}(x,0) = \left\{
\begin{array}{lll}
\mathbf{Q}_L(x_{i+1/2}, y_\alpha, z_\beta) & \text{if} & x < x_{i+1/2}, \\[2mm]
\mathbf{Q}_R(x_{i+1/2}, y_\alpha, z_\beta) & \text{if} & x > x_{i+1/2},
\end{array}
\right.
\end{array}
\right\}
\tag{19}
$$

To evaluate higher-order terms we first express all time derivatives by spatial derivatives by means of the Cauchy-Kowalewski procedure. We note that this procedure will now involve x, y and z derivatives up to order $r-1$. For the system in conservation form (13) we have

$$
\begin{aligned}
\partial_t \mathbf{Q} &= -\left(\frac{\partial \mathbf{F}}{\partial \mathbf{Q}}\right) \partial_x \mathbf{Q} - \left(\frac{\partial \mathbf{G}}{\partial \mathbf{Q}}\right) \partial_y \mathbf{Q} - \left(\frac{\partial \mathbf{H}}{\partial \mathbf{Q}}\right) \partial_z \mathbf{Q}, \\[2mm]
\partial_{tx} \mathbf{Q} &= -\left(\frac{\partial^2 \mathbf{F}}{\partial \mathbf{Q^2}}\right)(\partial_x \mathbf{Q})^2 - \left(\frac{\partial \mathbf{F}}{\partial \mathbf{Q}}\right)\partial_{xx}\mathbf{Q} - \left(\frac{\partial^2 \mathbf{G}}{\partial \mathbf{Q^2}}\right)(\partial_x \mathbf{Q})(\partial_y \mathbf{Q}) - \left(\frac{\partial \mathbf{G}}{\partial \mathbf{Q}}\right)\partial_{xy}\mathbf{Q} \\[2mm]
&\quad -\left(\frac{\partial^2 \mathbf{H}}{\partial \mathbf{Q^2}}\right)(\partial_x \mathbf{Q})(\partial_z \mathbf{Q}) - \left(\frac{\partial \mathbf{H}}{\partial \mathbf{Q}}\right)\partial_{xz}\mathbf{Q}, \\[2mm]
\partial_{ty} \mathbf{Q} &= -\left(\frac{\partial^2 \mathbf{F}}{\partial \mathbf{Q^2}}\right)(\partial_y \mathbf{Q})(\partial_x \mathbf{Q}) - \left(\frac{\partial \mathbf{F}}{\partial \mathbf{Q}}\right)\partial_{xy}\mathbf{Q} - \left(\frac{\partial^2 \mathbf{G}}{\partial \mathbf{Q^2}}\right)(\partial_y \mathbf{Q})^2 - \left(\frac{\partial \mathbf{G}}{\partial \mathbf{Q}}\right)\partial_{yy}\mathbf{Q} \\[2mm]
&\quad -\left(\frac{\partial^2 \mathbf{H}}{\partial \mathbf{Q^2}}\right)(\partial_y \mathbf{Q})(\partial_z \mathbf{Q}) - \left(\frac{\partial \mathbf{H}}{\partial \mathbf{Q}}\right)\partial_{yz}\mathbf{Q}, \\[2mm]
\partial_{tz} \mathbf{Q} &= -\left(\frac{\partial^2 \mathbf{F}}{\partial \mathbf{Q^2}}\right)(\partial_z \mathbf{Q})(\partial_x \mathbf{Q}) - \left(\frac{\partial \mathbf{F}}{\partial \mathbf{Q}}\right)\partial_{xz}\mathbf{Q} - \left(\frac{\partial^2 \mathbf{G}}{\partial \mathbf{Q^2}}\right)(\partial_z \mathbf{Q})(\partial_y \mathbf{Q}) - \left(\frac{\partial \mathbf{G}}{\partial \mathbf{Q}}\right)\partial_{yz}\mathbf{Q} \\[2mm]
&\quad -\left(\frac{\partial^2 \mathbf{H}}{\partial \mathbf{Q^2}}\right)(\partial_z \mathbf{Q})^2 - \left(\frac{\partial \mathbf{H}}{\partial \mathbf{Q}}\right)\partial_{zz}\mathbf{Q}, \\[2mm]
\partial_{tt} \mathbf{Q} &= -\left(\frac{\partial^2 \mathbf{F}}{\partial \mathbf{Q^2}}\right)(\partial_t \mathbf{Q})(\partial_x \mathbf{Q}) - \left(\frac{\partial \mathbf{F}}{\partial \mathbf{Q}}\right)\partial_{tx}\mathbf{Q} - \left(\frac{\partial^2 \mathbf{G}}{\partial \mathbf{Q^2}}\right)(\partial_t \mathbf{Q})(\partial_y \mathbf{Q}) - \left(\frac{\partial \mathbf{G}}{\partial \mathbf{Q}}\right)\partial_{ty}\mathbf{Q} \\[2mm]
&\quad -\left(\frac{\partial^2 \mathbf{H}}{\partial \mathbf{Q^2}}\right)(\partial_t \mathbf{Q})(\partial_z \mathbf{Q}) - \left(\frac{\partial \mathbf{H}}{\partial \mathbf{Q}}\right)\partial_{tz}\mathbf{Q}
\end{aligned}
\tag{20}
$$

and so on. An optimized FORTRAN or C output can be produced using algebraic manipulators and then can be directly included into the actual code.

Entirely analogous to the one-dimensional case, we can derive nonhomogeneous evolution equations and the initial conditions for each spatial derivative

$$
\mathbf{Q}^{(k+l+m)} \equiv \frac{\partial^{m+n+l}}{\partial x^m \partial y^n \partial z^l} \mathbf{Q}, \quad 1 \le m + n + l \le r - 1
$$

by differentiating the governing equation (13) and reconstruction polynomials $\mathbf{Q}_L$, $\mathbf{Q}_R$ with respect to x. The evolution equations have exactly the same form as (8) with a difference. The right hand side will now depend not only on lower order x derivatives but also on mixed derivatives. For the Taylor expansion (18) we need the values at $x = x_{i+1/2}$, $\tau = 0$. Therefore, entirely analogous to the one-dimensional case, we neglect the source

term, linearize the equation around the leading term of the time expansion (18) and replace the piece-wise polynomial initial data by the left and right extrapolated values. The spatial derivatives at $(x - x_{i+1/2})/\tau = 0$ are then the Godunov states of the following linearised Riemann problem with piece-wise constant initial data:

$$\partial_t \left(\mathbf{Q}^{(k+l+m)} \right) + \mathbf{A}_{i+1/2}\, \partial_x \left(\mathbf{Q}^{(k+l+m)} \right) = 0, \quad \mathbf{A}_{i+1/2} = \mathbf{A}(\mathbf{Q}(x_{i+1/2}, y_\alpha, z_\beta, 0+)),$$

$$\mathbf{Q}^{(k+l+m)} = \begin{cases} \dfrac{\partial^{m+n+l}}{\partial x^m \partial y^n \partial z^l} \mathbf{Q}_L(x_{i+1/2}, y_\alpha, z_\beta), & x < x_{i+1/2} \\[2mm] \dfrac{\partial^{m+n+l}}{\partial x^m \partial y^n \partial z^l} \mathbf{Q}_R(x_{i+1/2}, y_\alpha, z_\beta), & x > x_{i+1/2} \end{cases} \qquad (21)$$

After solving (21) for $1 \le m + n + l \le r - 1$ we form the Taylor expansion (18) for the interface state at the Gaussian integration point $(x_{i+1/2}, y_\alpha, z_\beta)$. The flux of *the state-expansion* ADER scheme is obtained by inserting the approximate state (18) into formula (17) and using an appropriate r^{th}-order accurate quadrature for time integration:

$$\mathbf{F}_{i+1/2,jk} = \sum_{\alpha=1}^{N} \sum_{\beta=1}^{N} \left(\sum_{l=1}^{N} \mathbf{F}(\mathbf{Q}(x_{i+1/2}, y_\alpha, z_\beta, \tau_l)) K_l \right) K_\beta\, K_\alpha. \qquad (22)$$

For the *flux expansion* ADER schemes we write Taylor time expansion of the physical flux at each point $(x_{i+1/2},\, y_\alpha,\, z_\beta)$

$$\mathbf{F}(x_{i+1/2}, y_\alpha, z_\beta, \tau) = \mathbf{F}(x_{i+1/2}, y_\alpha, z_\beta, 0+) + \sum_{k=1}^{r-1} \left[\frac{\partial^k}{\partial t^k} \mathbf{F}(x_{i+1/2}, y_\alpha, z_\beta, 0+) \right] \frac{\tau^k}{k!}. \qquad (23)$$

From (16) and (23) the numerical flux is given by

$$\mathbf{F}_{i+1/2,jk} = \sum_{\alpha=1}^{N} \sum_{\beta=1}^{N} \left(\mathbf{F}(x_{i+1/2}, y_\alpha, z_\beta, 0+) + \sum_{k=1}^{r-1} \left[\frac{\partial^k}{\partial t^k} \mathbf{F}(x_{i+1/2}, y_\alpha, z_\beta, 0+) \right] \frac{\Delta t^k}{(k+1)!} \right) K_\alpha K_\beta. \qquad (24)$$

Entirely analogous to the one-dimensional case, the leading term $\mathbf{F}(x_{i+1/2}, y_\alpha, z_\beta, 0+)$ is computed from (19) using a monotone upwind flux. The remaining higher order time derivatives of the flux in (23) are expressed via time derivatives of the intercell state $\mathbf{Q}(x_{i+1/2}, y_\alpha, z_\beta, \tau)$ which are given by the Taylor expansion (18).

The solution is advanced in time by updating the cell averages according to the one-step formula (14).

4 Numerical results

In this section we present numerical results of the ADER schemes as applied to the multidimensional compressible Euler equations of the form (13) with

$$\mathbf{Q} = \begin{pmatrix} \rho \\ \rho u \\ \rho v \\ \rho w \\ E \end{pmatrix}, \quad \mathbf{F} = \mathbf{Q}u + \begin{pmatrix} 0 \\ p \\ 0 \\ 0 \\ pu \end{pmatrix}, \quad \mathbf{G} = \mathbf{Q}v + \begin{pmatrix} 0 \\ 0 \\ p \\ 0 \\ pv \end{pmatrix}, \quad \mathbf{H} = \mathbf{Q}w + \begin{pmatrix} 0 \\ 0 \\ 0 \\ p \\ pw \end{pmatrix}, \qquad (25)$$

$$p = (\gamma - 1)(E - \frac{1}{2}\rho(u^2 + v^2 + w^2)).$$

Here ρ, u, v, w p and E are density, components of velocity in the x, y and z coordinate directions, pressure and total energy, respectively; γ is the ratio of specific heats. We use $\gamma = 1.4$ throughout.

The state-expansion ADER schemes need the Godunov state of the Riemann problems (6), (19) to provide the leading term of the state expansions (5), (18) respectively. In general, any exact or approximate Riemann solver can be used for this purpose. In this paper we choose the adaptive Riemann solver described of Sect. 9.5.2 of [29]. We remark that the computational cost of the Riemann solver is very small compared to the overall cost of the scheme, typically around 5%. Other parts of the schemes are considerably more expensive, e.g. the reconstruction procedure takes around 60% of the computing time.

The flux-expansion ADER schemes additionally need a first-order upwind flux to provide the leading term of the flux expansions (12),(24). We have successfully used a number of upwind fluxes, including the Rusanov flux [19], the Roe flux [18], the HLL flux [9], the HLLC flux [36] and a very recent multistage MUSTA flux [35]. For general background on the fluxes see also [29]. However, the aim of this paper is not to assess the performance of different fluxes in the ADER framework. Rather we would like to illustrate the idea of the flux-expansion ADER schemes. Therefore, we present results for only two numerical fluxes, the HLL flux and HLLC fluxes. The HLL flux assumes a two-wave structure of the Riemann problem solution with wave speeds S_L and S_R. The HLLC fluxes uses a more accurate three-wave structure, which includes the middle wave with the speed S_*. These wave speeds must be estimated. We use the pressure-velocity estimates of Sect. 10.5.2 of [29].

For both state-expansion and flux-expansion variants of the ADER approach we use the fourth-order Simpson rule for time integration in (10), (22).

We denote the state-expansion ADER schemes of third and fourth orders of time accuracy, using the adaptive Riemann solver from [29], as ADER3-AD and ADER4-AD respectively. The corresponding flux expansion ADER schemes are denoted as ADER3-HLLC, ADER4-HLLC (the HLLC flux is used) and ADER3-HLL and ADER4-HLL (the HLL flux is used).

For comparisons in our numerical experiments we also run the dimension-by-dimension version of the finite-volume WENO scheme of Shi, Hu and Shu [22]. The WENO scheme uses the piece-wise parabolic ($r = 3$) reconstruction, three-point (sixth order) Gaussian rule for flux integration, the Rusanov flux [19] as a building block and the third order TVD Runge-Kutta method for time discretization [23]. Therefore it is formally fifth order accurate in space and third order accurate in time.

In our computations we evaluate a stable time step Δt according to

$$\Delta t = C_{cfl} \times \min_{ijk} \left(\frac{\Delta x}{|S_{ijk}^{n,x}|}, \frac{\Delta y}{|S_{ijk}^{n,y}|}, \frac{\Delta z}{|S_{ijk}^{n,z}|} \right). \tag{26}$$

Here $S_{ijk}^{n,d}$ is the speed of the fastest wave present at time level n travelling in the d direction, with $d = x, y, z$. C_{cfl} is the CFL number and is chosen according to the linear stability condition of the scheme, namely $0 < C_{cfl} \leq 1/2$ in two space dimensions and

$0 < C_{cfl} \leq 1/3$ in three space dimensions. We run all convergence tests with a fixed Courant number close to the stability limit. Usually we use $C_{cfl} = 0.45$ in two space dimensions and $C_{cfl} = 0.3$ in three space dimensions.

We remark that the ADER3-AD, ADER3-HLLC and ADER3-HLL schemes of the present paper and the WENO scheme [22] use the same piece-wise parabolic ($r = 3$) reconstruction. Therefore, their comparison is indeed justified. The fourth-order ADER4 and ADER4-HLL schemes use more accurate piece-wise cubic ($r = 4$) WENO reconstruction; therefore their comparison with other schemes must be qualified.

We assess performance our methods as applied to the following test problems.

4.1   Two-dimensional vortex evolution problem

We solve the two-dimensional Euler equations in the square domain $[-5 : 5] \times [-5 : 5]$ with periodic boundary conditions. The initial condition corresponds to a smooth vortex placed at the origin and is defined as the following isentropic perturbation to the uniform flow of unit values of primitive variables [1]:

$$u = 1 - \frac{\varepsilon}{2\pi} e^{\frac{1}{2}(1-r^2)} y, \quad v = 1 + \frac{\varepsilon}{2\pi} e^{\frac{1}{2}(1-r^2)} x,$$
$$T = 1 - \frac{(\gamma-1)\varepsilon^2}{8\gamma\pi^2} e^{(1-r^2)}, \quad \frac{p}{\rho^\gamma} = 1, \tag{27}$$

where $r^2 = x^2 + y^2$ and the vortex strength is $\varepsilon = 5$. The exact solution is a vortex movement with a constant velocity at 45° to the Cartesian mesh lines. We compute the numerical solution at the output time $t = 10$ for which the vortex returns to the initial position. We use $C_{cfl} = 0.45$ for all runs.

Table 1 shows the convergence study for the ADER and WENO schemes with the piece-wise parabolic ($r = 3$) reconstruction. We present errors and convergence rates in L_∞ and L_1 norm for cell averages of density. We observe that the ADER schemes achieve approximately sixth and fifth orders of accuracy in L_∞ and L_1 norms respectively. It is interesting to note that these orders of accuracy actually exceed the fourth order accuracy of the two-point Gaussian rule used for flux integration. The WENO scheme is less accurate than the ADER schemes by a factor of two on coarse meshes and by a factor of three on the finest mesh.

Table 2 shows the convergence study for the fourth order ADER schemes with the higher-order piece-wise cubic ($r = 4$) reconstruction. We observe that approximately sixth order of accuracy in both norms. For a fixed resolution the fourth order ADER schemes are more accurate than the schemes of Table 1 by a factor of ten.

We also note, that the accuracy of the ADER-AD and ADER-HLLC schemes of the same order is very similar whereas the ADER-HLL schemes are slightly less accurate.

4.2   Double Mach reflection of a strong shock

The setup of the problem is as follows [37]. The domain of interest is a region of 4 units long and 1 unit wide. At the initial time $t = 0$ a right-moving shock wave of shock Mach number equal to 10 is set up. The shock front makes an angle of 60° with the

Table 1: Density convergence study for the vortex evolution problem (27) at the output time $t = 10$. ADER and WENO schemes with piece-wise parabolic ($r = 3$) reconstruction.

Method	Mesh	L_∞ error	L_∞ order	L_1 error	L_1 order
ADER3-AD	25×25	5.94×10^{-2}		3.43×10^{-1}	
	50×50	8.90×10^{-3}	2.74	2.50×10^{-2}	3.78
	100×100	2.62×10^{-4}	5.08	8.83×10^{-4}	4.82
	200×200	4.55×10^{-6}	5.85	3.58×10^{-5}	4.62
ADER3-HLLC	25×25	5.94×10^{-2}		3.43×10^{-1}	
	50×50	8.94×10^{-3}	2.73	2.50×10^{-2}	3.78
	100×100	2.63×10^{-4}	5.09	8.83×10^{-4}	4.82
	200×200	4.68×10^{-6}	5.81	3.61×10^{-5}	4.61
ADER3-HLL	25×25	6.08×10^{-2}		3.87×10^{-1}	
	50×50	9.32×10^{-3}	2.71	2.64×10^{-2}	3.88
	100×100	2.86×10^{-4}	5.02	9.97×10^{-3}	4.73
	200×200	4.90×10^{-6}	5.87	3.79×10^{-5}	4.72
WENO [22]	25×25	1.04×10^{-1}		6.92×10^{-1}	
	50×50	1.38×10^{-2}	2.91	4.58×10^{-2}	3.92
	100×100	4.60×10^{-4}	4.91	2.33×10^{-3}	4.30
	200×200	1.67×10^{-5}	4.78	9.05×10^{-5}	4.68

x-axis at $x = 1/6$. Ahead of the shock the gas is at rest with $\rho = 1.4$, $p = 1$. The following boundary conditions are used. The in-flow boundary condition is applied at the left vertical boundary $x = 0$ and transmissive boundary conditions are used at the right vertical boundary $x = 4$. At the bottom boundary $y = 0$ the exact post-shock values of all gas parameters are set for $0 \le x \le 1/6$ whereas for $1/6 < x \le 4$ reflective boundary conditions are used. The exact motion of the Mach 10 shock is prescribed at the top boundary $y = 1$. The solution is studied for the output time $t = 1/5$.

Figs. 1–6 show numerical results of third-order ADER3-AD, ADER3-HLLC and ADER3-HLL schemes for three meshes: 480×120, 960×240 and 1920×480 cells. The corresponding results of the WENO scheme can be found in Fig. 3.4 of [22] and are not shown here. Comparing our results with those in the existing literature [37, 10, 4, 8, 22] it is seen that ADER schemes produce the flow pattern generally accepted at present as corrected, on all meshes. All discontinuities are well resolved and correctly positioned. Comparing our new schemes, ADER3-AD, ADER3-HLLC, ADER3-HLL, and the WENO scheme [22], we see that the main difference occurs in the resolution of the slip surfaces and the associated jet. This is partly explained by the numerical flux. The adaptive Riemann solver used to compute the leading term of the state expansion (18) in the ADER3 scheme and the HLLC Riemann solver used for the leading term of the flux expansion (24) in the ADER3-HLLC scheme recognize all these waves. In fact, the numerical results of
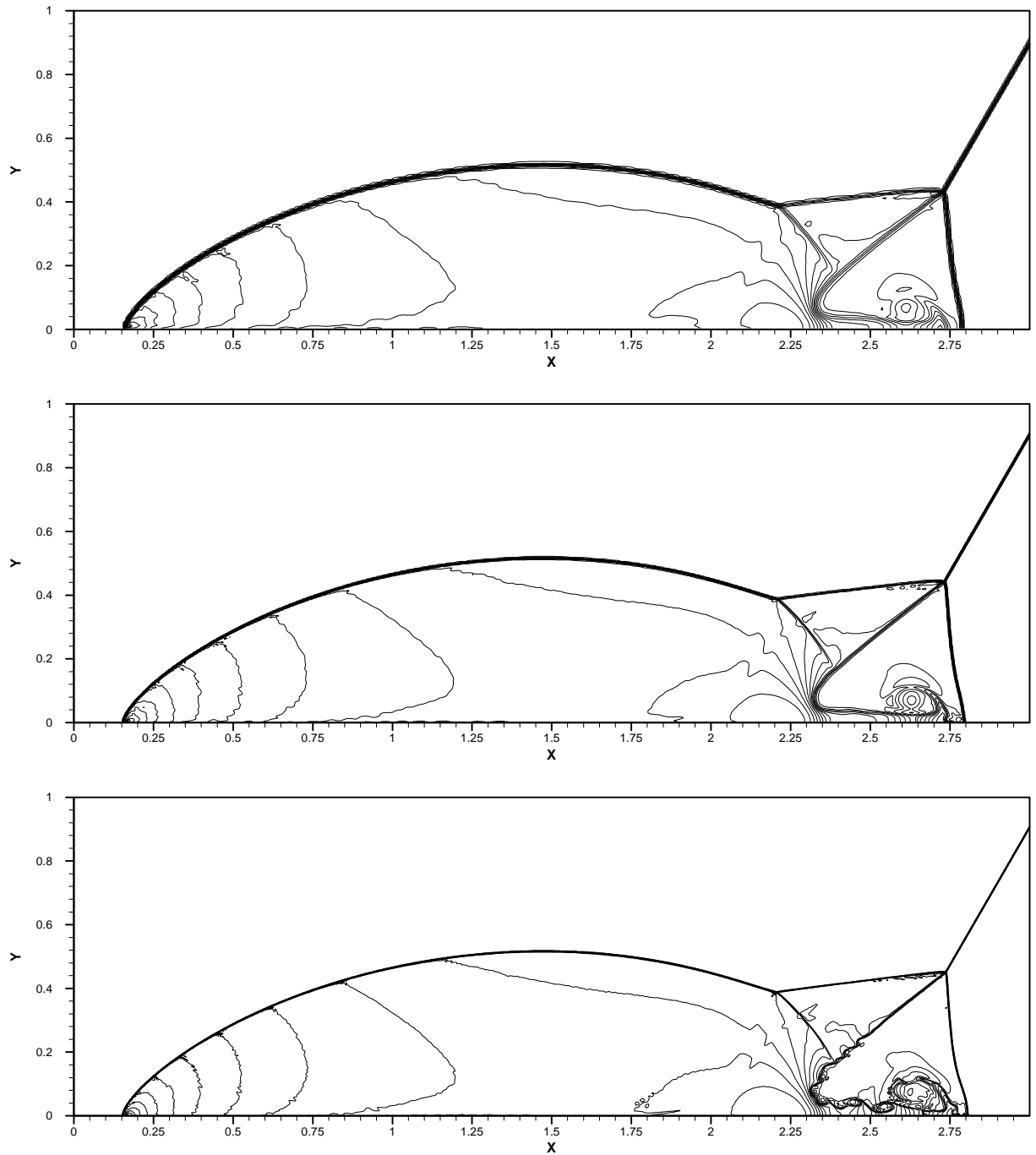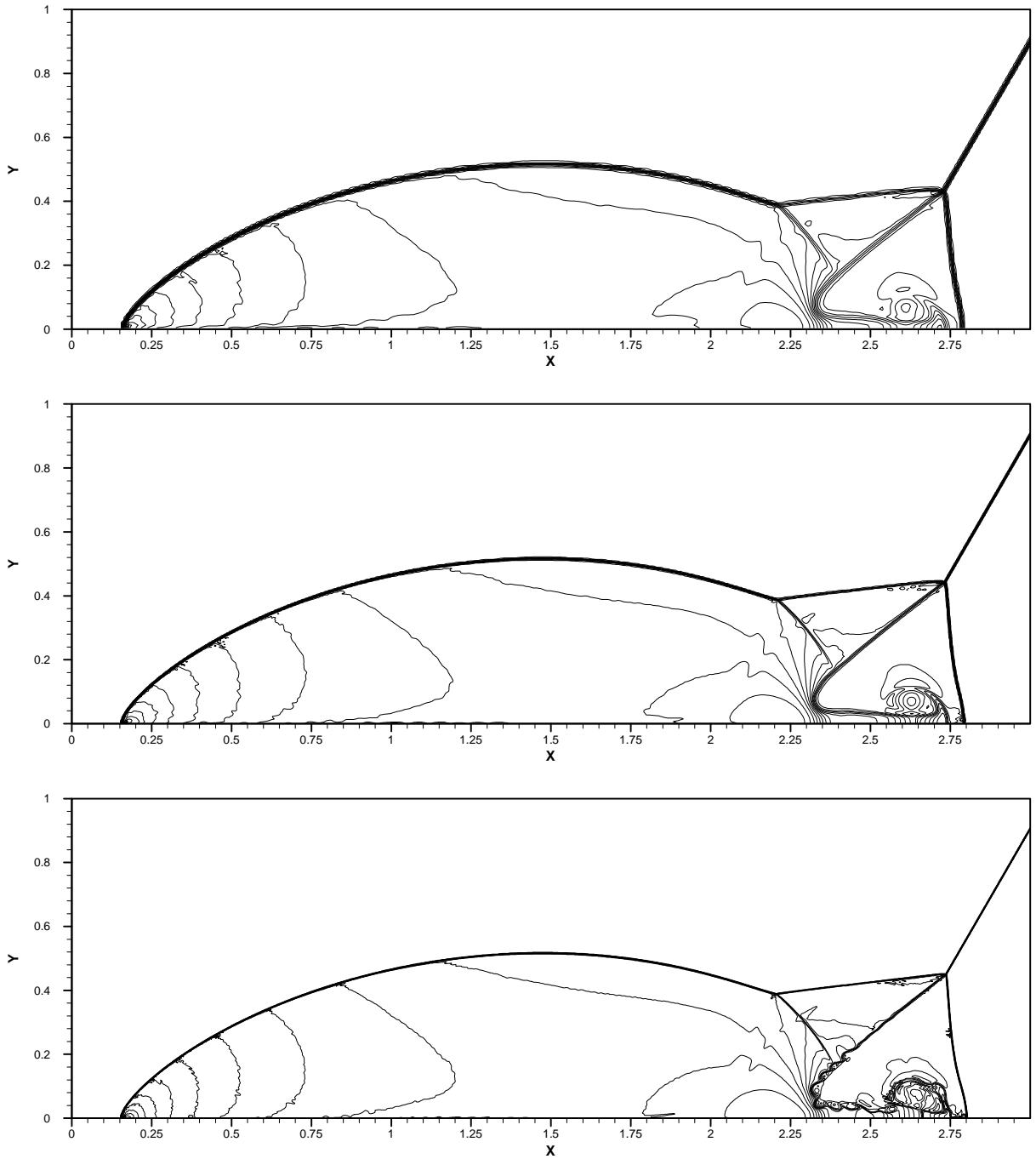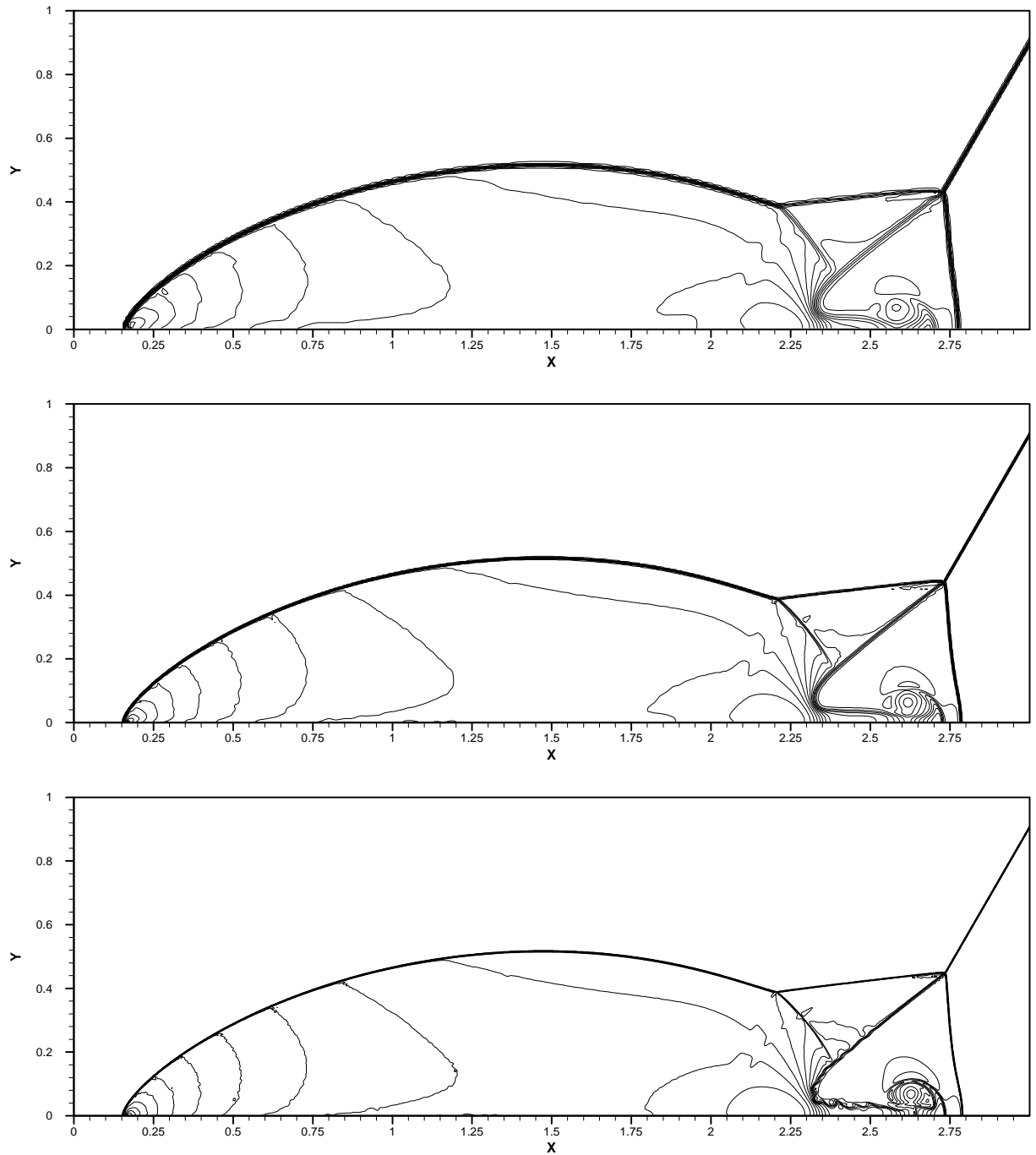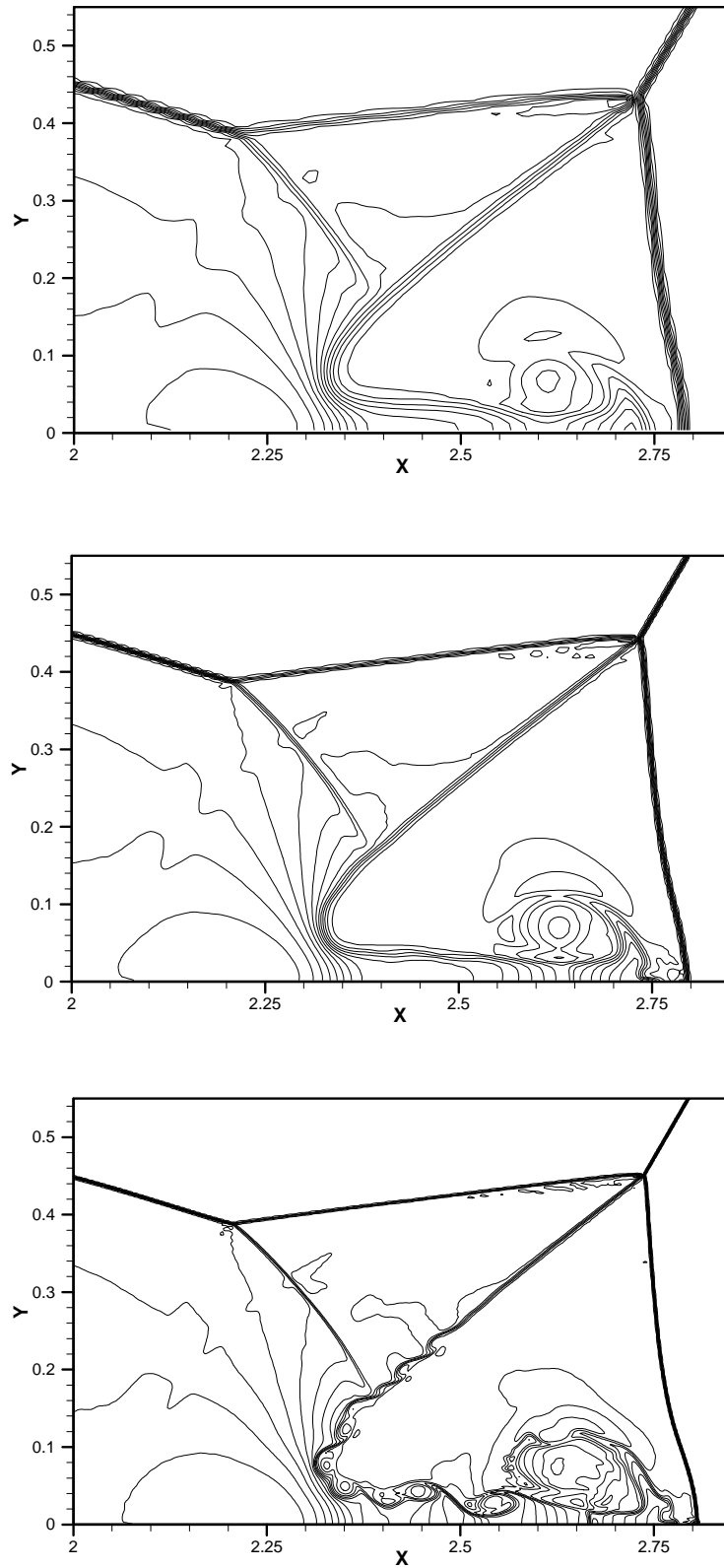
Figure 1: Density convergence study for the double Mach reflection problem. Method: the ADER3-AD scheme. Meshes: 480×120 cells (top) , 960×240 cells (middle) and 1920×480 cells (bottom). 30 contour lines from 2 to 22.
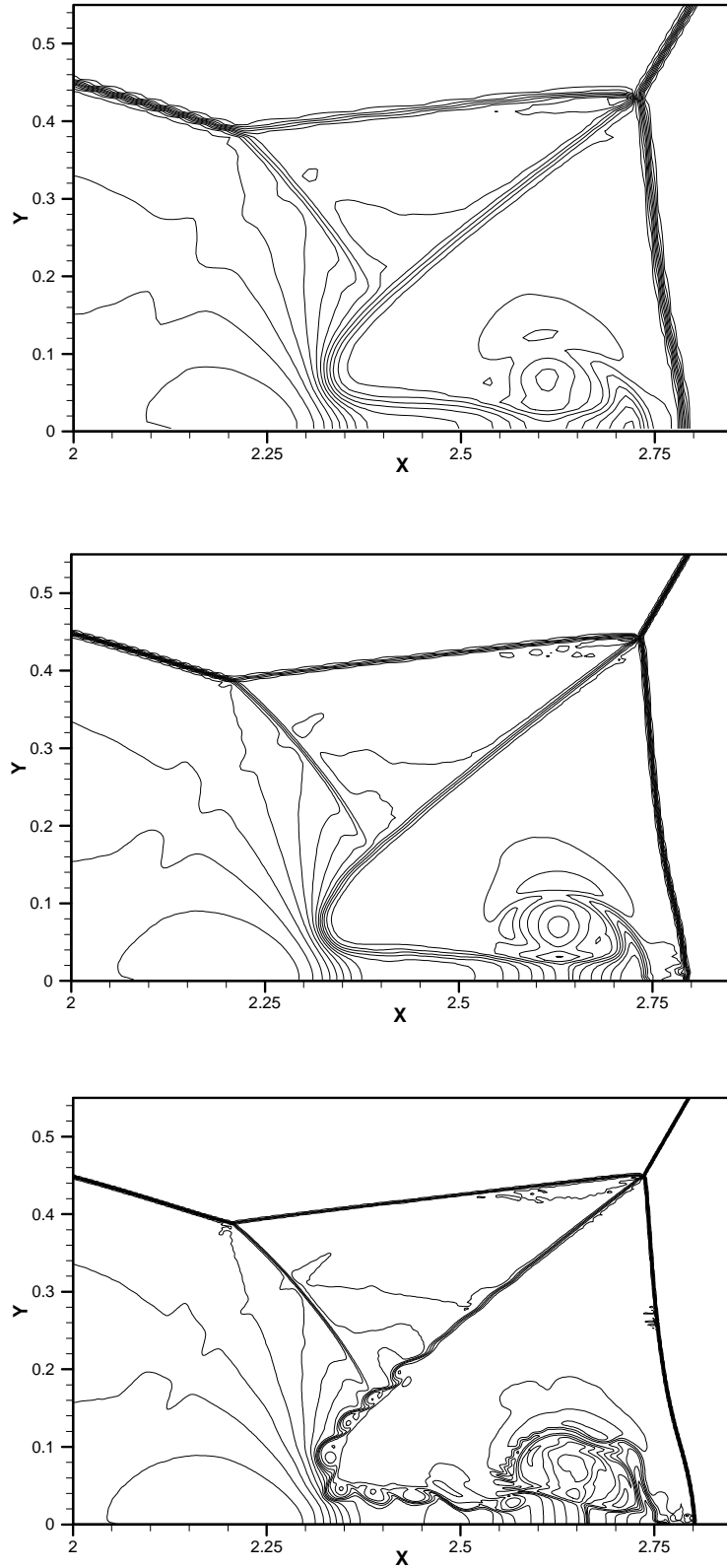
12

Figure 2: Density convergence study for the double Mach reflection problem. Method: the ADER3-HLLC scheme. Meshes: 480×120 cells (top) , 960×240 cells (middle) and 1920×480 cells (bottom). 30 contour lines from 2 to 22.

Figure 3: Density convergence study for the double Mach reflection problem. Method: the ADER3-HLL scheme. Meshes: 480×120 cells (top) , 960×240 cells (middle) and 1920×480 cells (bottom). 30 contour lines from 2 to 22.
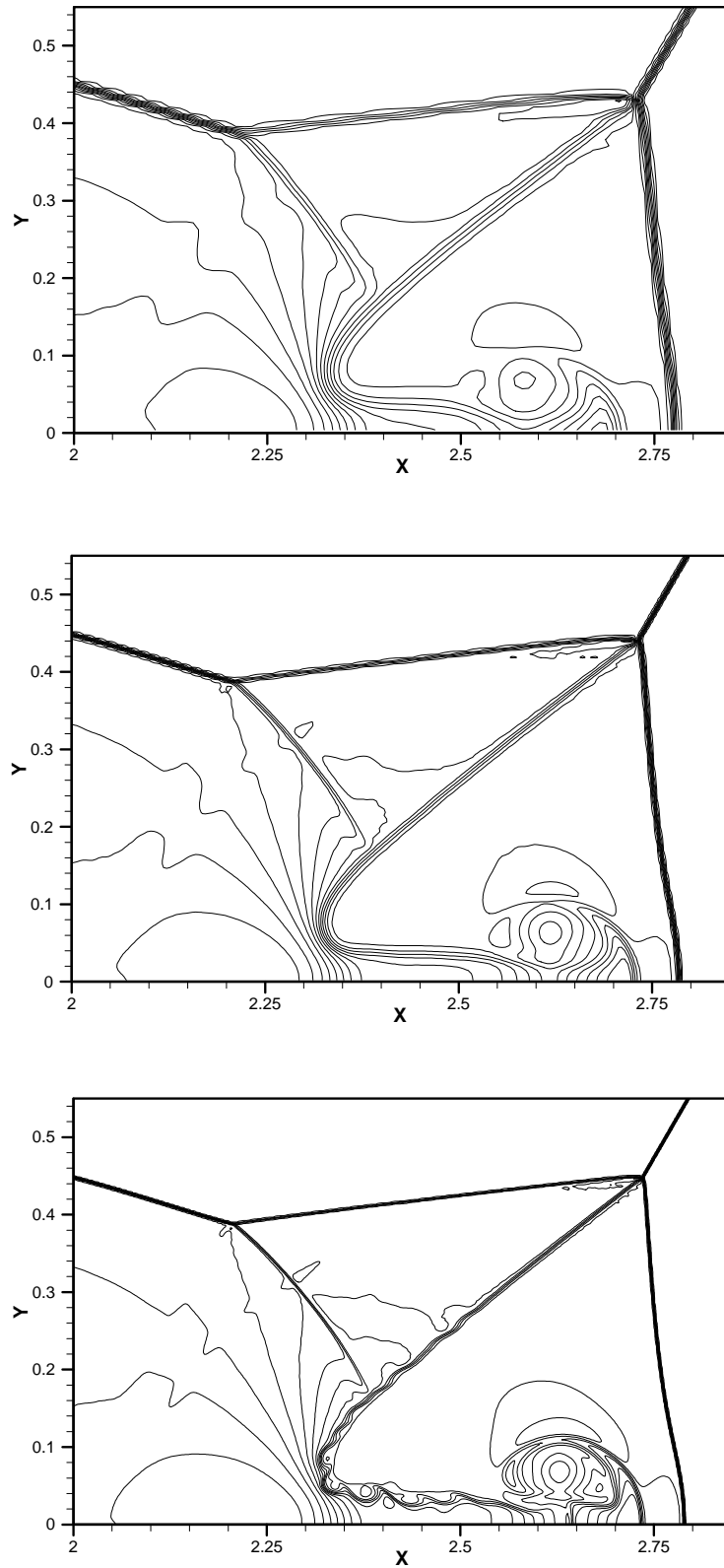
Figure 4: Density convergence study for the double Mach reflection problem. Method: the ADER3-AD scheme. Meshes: 480×120 cells (top) , 960×240 cells (middle) and 1920×480 cells (bottom). 30 contour lines from 2 to 22. Zoomed area of Fig. 1.
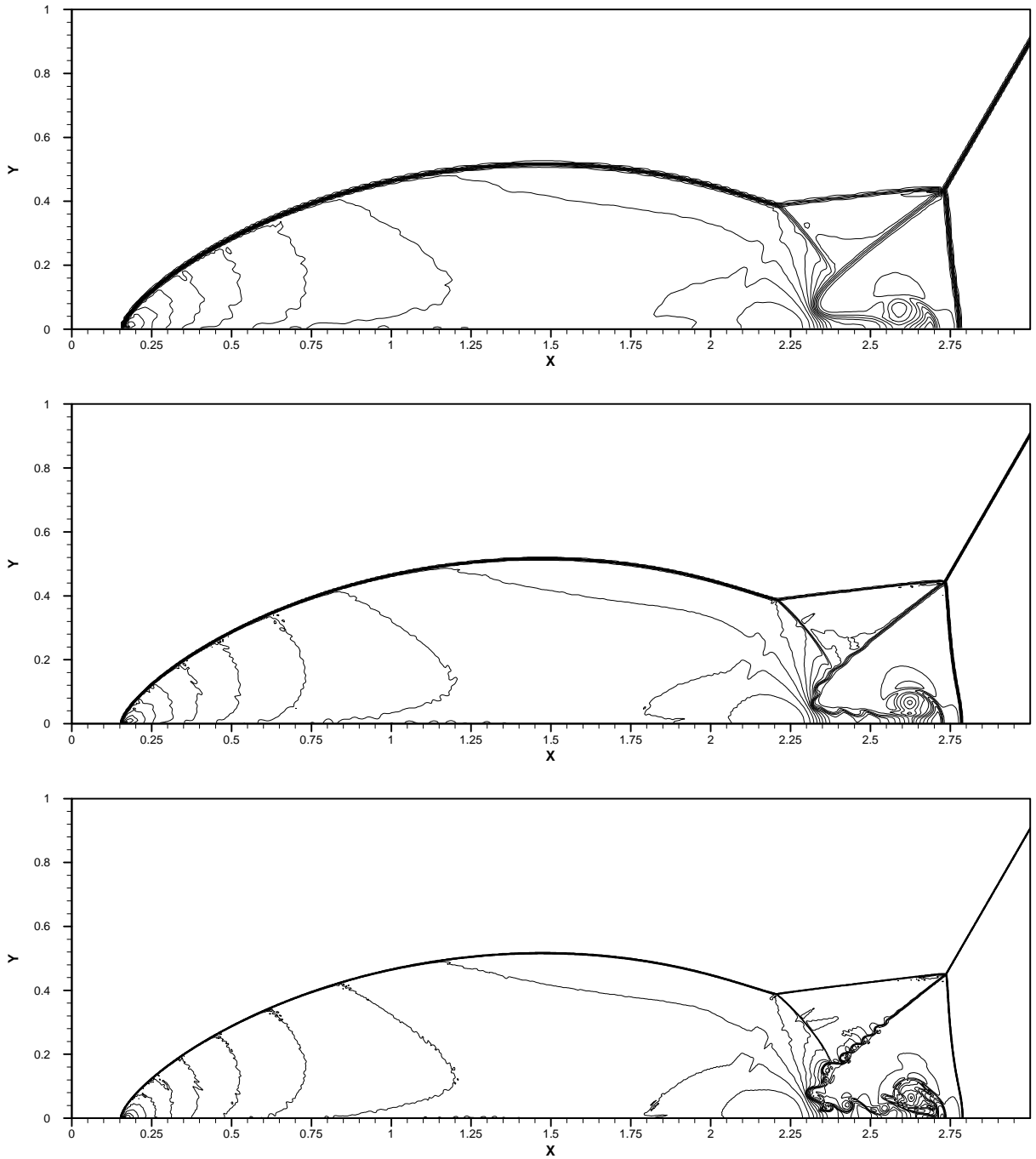
15

Figure 5: Density convergence study for the double Mach reflection problem. Method: the ADER3-HLLC scheme. Meshes: 480×120 cells (top) , 960×240 cells (middle) and 1920×480 cells (bottom). 30 contour lines from 2 to 22. Zoomed area of Fig. 2

16

Figure 6: Density convergence study for the double Mach reflection problem. Method: the ADER3-HLL scheme. Meshes: 480×120 cells (top) , 960×240 cells (middle) and 1920×480 cells (bottom). 30 contour lines from 2 to 22. Zoomed area of Fig. 3
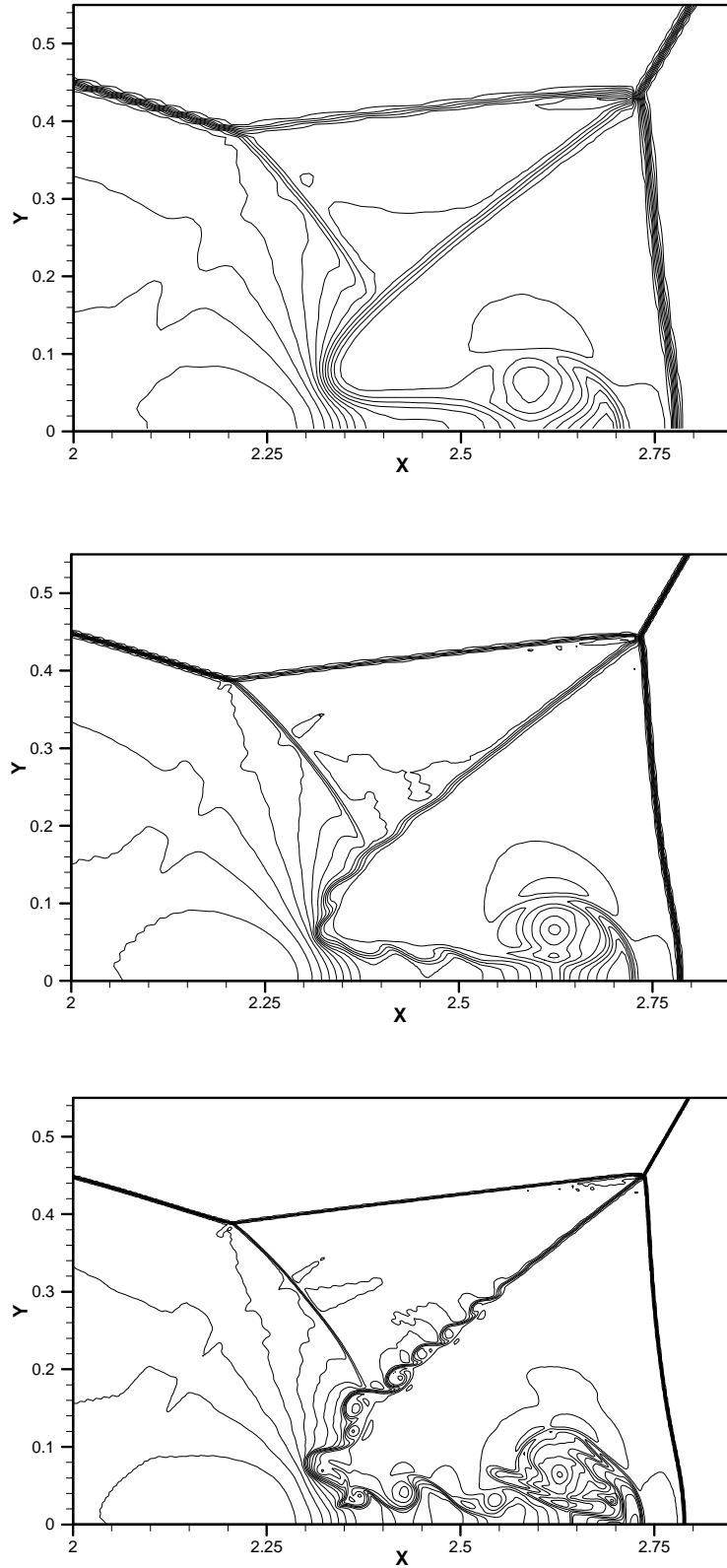
Figure 7: Density convergence study for the double Mach reflection problem. Method: the ADER4-HLL scheme. Meshes: 480×120 cells (top) , 960×240 cells (middle) and 1920×480 cells (bottom). 30 contour lines from 2 to 22.

Figure 8: Density convergence study for the double Mach reflection problem. Method: the ADER4-HLL scheme. Meshes: 480×120 cells (top) , 960×240 cells (middle) and 1920×480 cells (bottom). 30 contour lines from 2 to 22. Zoomed area of Fig. 7

Table 2: Density convergence study for the vortex evolution problem (27) at the output time $t = 10$. ADER schemes with piece-wise cubic ($r = 4$) reconstruction

Method	Mesh	L_∞ error	L_∞ order	L_1 error	L_1 order
ADER4-AD	25×25	1.96×10^{-2}		1.15×10^{-1}	
	50×50	1.59×10^{-3}	3.62	5.43×10^{-3}	4.40
	100×100	2.52×10^{-5}	5.98	1.29×10^{-4}	5.39
ADER4-HLLC	25×25	1.96×10^{-2}		1.15×10^{-1}	
	50×50	1.60×10^{-3}	3.62	5.43×10^{-3}	4.40
	100×100	2.52×10^{-5}	5.98	1.29×10^{-4}	5.40
ADER4-HLL	25×25	1.90×10^{-2}		1.15×10^{-1}	
	50×50	1.61×10^{-3}	3.56	5.68×10^{-3}	4.34
	100×100	2.79×10^{-5}	5.85	1.44×10^{-4}	5.31

the ADER3-AD and ADER3-HLLC schemes are very similar, almost identical. The HLL and the Rusanov fluxes used in the ADER3-HLL and the WENO schemes ignore the internal structure of the Riemann problem solution and thus smear the slip surfaces more significantly.

Additionally, we observe that all ADER schemes produce much sharper profiles of the shock waves as compared with the WENO scheme [22]. Presumably, this should be attributed to the one-step framework of the ADER approach.

On the finest mesh we begin to see the appearance of the Kelvin-Helmholtz instability (rolling) of the slip surface. We remark that slip surfaces are physically unstable features of the flow, the converged solution of which can only be obtained by solving the Navier-Stokes equations. See e.g. [38] for numerical study of two-dimensional Rayleigh-Taylor instability. When we use the Euler equations, the viscosity is in fact the numerical viscosity of the method and depends on *the scheme and the mesh* used. As the mesh is refined, no limiting (converged) solution is found. However, for a given particular mesh the numerical solution may exhibit features, typical of physically unstable flows, but with unknown viscosity. Therefore, more pronounced instability of the solution (rolling of the slip surfaces) means smaller numerical diffusion of the ADER3-AD and ADER3-HLLC schemes as compared to the ADER3-HLL scheme and the WENO scheme of [22].

Figs. 7–8 show numerical results of the higher-order ADER4-HLL scheme for the same meshes. We observe that the scheme produces the correct flow pattern on all meshes, with thin profiles of discontinuities. Comparing Fig. 8 with that of methods with the lower-order piece-wise parabolic reconstruction (see Figs. 1–6 and [22]) it is seen that the rolling of slip surfaces is much more pronounced in the results of ADER4-HLL scheme. Therefore, the ADER4-HLL scheme has significantly smaller numerical diffusion as compared with the lower-order schemes.

4.3 Three-dimensional explosion test problem

Finally, we apply our schemes to the three-dimensional Euler equations (25) and solve the spherical explosion test problem [29]. The initial condition defined on $[-1:1] \times [-1:1] \times [-1:1]$ consists of two regions of constant but different values of gas parameters separated by a sphere of radius 0.4:

$$(\rho, p) = \begin{cases} (1.0, \ 1.0), & r \leq 0.4 \\ (0.125, \ 0.1), & r > 0.4 \end{cases}, \quad u = v = w = 0, \quad r^2 = x^2 + y^2 + z^2. \tag{28}$$

The numerical solution is computed at the output time $t = 0.25$ on a mesh of 101 cells in each coordinate direction. We use $C_{cfl} = 0.3$ for all runs.
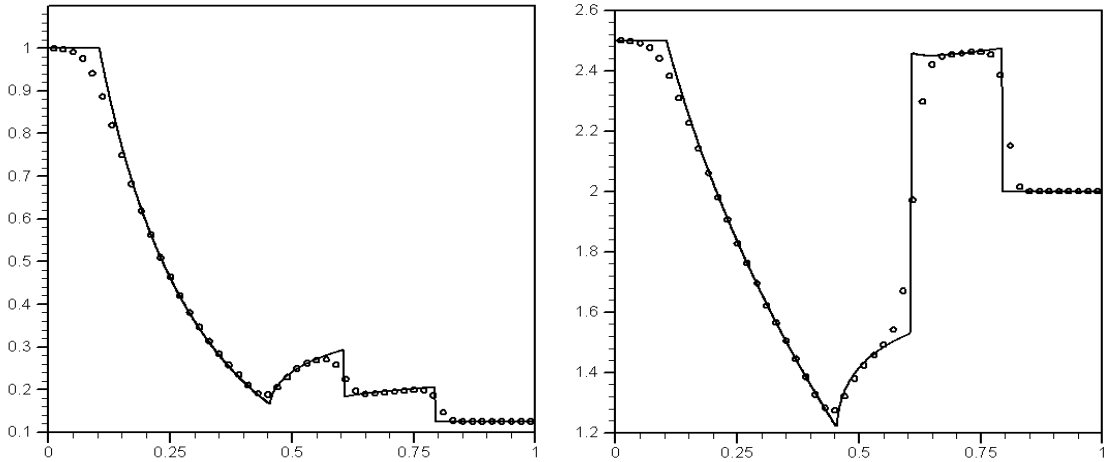
Figure 9: The spherical explosion test problem. Computed (symbol) and reference (line) solutions for density (left) and internal energy (right) for the ADER3-AD scheme. A mesh of $101 \times 101 \times 101$ cells is used.

Fig. 9 shows a comparison between the one-dimensional reference radial solution (solid line) and the cell averages of the three-dimensional ADER3-AD solution (symbols) along the radial line that is coincident with the x-axis. We present distributions of gas density ρ and internal energy e for $x > 0$. The solution contains a spherical shock wave and a contact surface travelling away from the centre and a spherical rarefaction wave travelling towards the origin (0,0,0). We observe that the scheme produce the correct flow patter with the correct values behind the shock wave and the contact surface. No oscillations are present.

The results of the ADER3-HLLC and ADER3-HLL schemes are essentially the same and are thus omitted.

4.4 Cost comparison of the schemes

Our numerical experiments show that for the two-dimensional compressible Euler equations and piece-wise parabolic reconstruction the third-order ADER schemes are faster than the WENO scheme roughly by 70%. The reason for this is twofold. Firstly, our scheme needs to perform the very costly characteristic projections and smoothness indicators computations in the reconstruction procedure only once during the time step.

Secondly, the ADER schemes uses the two-point integration rule to evaluate the numerical fluxes whereas the WENO scheme in the cited reference uses the three-point Gaussian rule.

The gain in computational cost of ADER schemes over the WENO schemes with Runge-Kutta time stepping is similar to that of the finite-difference WENO schemes with Cauchy-Kowalewski procedure over the finite-difference WENO schemes with Runge-Kutta time stepping [17].

The fourth order ADER schemes in two space dimensions are more expensive than the corresponding third order ADER schemes by a factor of three. This is due to substantially more expensive reconstruction procedure and more complicated fluxes.

Secondly, we discuss the memory requirement of the schemes. The ADER schemes of any order effectively need only two global arrays to store the vector of the conservative variables and the total sum of fluxes. The WENO schemes with the third order three-stage TVD Runge-Kutta method [23] need at least three such arrays. Note that expensive memory transfers may be needed for the RK method in this case. For the fourth order *five stage* SSP RK method [24] the memory requirements are substantially higher. Therefore, the memory requirement of the ADER schemes are significantly smaller than that of the WENO schemes with RK time discretizations.

5   Conclusions

In this paper we have extended the ADER approach to multidimensional nonlinear systems of conservation laws. We implemented schemes of third and fourth order of time accuracy as applied to the compressible Euler equations of gas dynamics in two and three space dimensions. We presented the numerical results which illustrate their very high order of accuracy as well as essentially non-oscillatory property of the schemes. Comparisons with the state-of-art WENO scheme [22] show that the ADER schemes are faster, more accurate and need less computer memory.

References

[1] Balsara D.S. and Shu C.W. (2000). Monotonicity preserving weighted essentially non-oscillatory schemes with increasingly high order of accuracy. *J. Comput. Phys*, **160**, pp. 405-452.

[2] Ben-Artzi M. and Falcovitz J. (1984). A Second–Order Godunov–Type Scheme for Compressible Fluid Dynamics. *J. Comp. Phys.*, **55**, 1–32.

[3] Casper J. and Atkins H. (1993). A finite-volume high order ENO scheme for two dimensional hyperbolic systems. *J. Comput. Phys.*, **106**, pp. 62-76.

[4] Cockburn B. and Shu C.-W. (2001) Runge-Kutta discontinuous Galerkin methods for convection-dominated problems. *J. Sci. Comput.*, **16** , pp. 173-261.

[5] Godunov SK. (1959). A finite difference method for the computation of discontinuous solutions of the equations of fluid dynamics. *Mat. Sbornik*, **47**, pp. 357-393.

[6] Godunov S.K., Zabrodin A.V., Ivanov M.Y., Kraiko A.N. and Prokopov G.P. *Numerical solution of multi-dimensional problems in gas dynamics*. Nauka Press, Moscow, 1976 (in Russian).

[7] Godunov S., Zabrodin A. , Ivanov M.Y., Kraiko A.N. and Prokopov G.P. *Resolution Numerique des Problemes Multidimensionnels de la Dinamique des Gaz*, Moscow; Mir 1979. 414 p.

[8] Hu C. and Shu C.-W. (1999). Weighted essentially non-oscillatory schemes on triangular meshes. *J. Comput. Phys.*, **150**, pp. 97-127.

[9] Harten A. , Lax P. D. and van Leer B. (1983). On upstream differencing and Godunov-type schemes for hyperbolic conservation laws. *SIAM Review*, **25**(1), pp. 35-61.

[10] Jiang G.S. and Shu C.W. (1996). Efficient implementation of weighted ENO schemes. *J. Comput. Phys.*, **126**, pp. 202–212.

[11] Käser M. (2003). ADER Schemes for the Solution of Conservation Laws on Adaptive Triangulations. Mathematical Methods and Modeling in Hydrocarbon Exploration and Production planned for publishing in the Springer-Verlag book series Mathematics in Industry. *to appear*

[12] Kolgan N.E. (1972). Application of the minimum-derivative principle in the construction of finite-difference schemes for numerical analysis of discontinuous solutions in gas dynamics. *Uchenye Zapiski TsaGI* [Sci. Notes of Central Inst. of Aerodynamics], **3**(6), pp. 68-77 (in Russian).

[13] Kolgan N.E. (1975). Finite-difference schemes for computation of three dimensional solutions of gas dynamics and calculation of a flow over a body under an angle of attack. *Uchenye Zapiski TsaGI* [Sci. Notes of Central Inst. of Aerodynamics], **6**(2), pp. 1-6 (in Russian).

[14] Men'shov I.S., (1990). Increasing the order of approximation of Godunov's scheme using solution of the generalized Riemann problem. *U.S.S.R. Comput. Math. Phys.*, **30**, No. 5, pp.54-65.

[15] Men'shov I.S., (1991). Generalized problem of break-up of a single discontinuity. *Prikl. Matem. i Mekhan.*, **55**, No. 1, pp.86-95 (*Journal of Applied Mathematics and Mechanics*).

[16] Men'shov I.S., (1992). Accuracy increase of the Godunov scheme for stationary supersonic Euler equations based on the solution of generalized Riemann problem. *U.S.S.R. Comput. Math. and Math. Phys.*, **32**, No. 2, pp.257-263.

[17] Qiu J. and Shu C.-W. (2003) Finite difference WENO schemes with Lax-Wendroff type time discretization. *SIAM J. Sci. Comput.*, **24**, pp.2185-2198.

[18] Roe P.L. (1981). Approximate Riemann solvers, parameter vectors, and difference schemes. *J. Comp. Phys.*, **43**, pp. 357-372.

[19] Rusanov V.V. (1961). Calculation of interaction of non-steady shock waves with obstacles. *J. Comp. Math. Phys., USSR*, **1**, pp. 267-279.

[20] Schwartzkopff T., Munz C.D. and Toro E.F. (2002) ADER-2D: a high-order approach for linear hyperbolic systems in 2D. *J. Sci. Comput.*, **17**, pp. 231-240.

[21] Schwartzkopff T., Dumbser M. and Munz C.D. (2004) Fast high order ADER schemes for linear hyperbolic equations. *J. Comput. Phys., in press.*

[22] Shi J., Hu C. and Shu C.-W. (2002). A technique for treating negative weights in WENO schemes. *J. Comput. Phys.*, **175**, pp. 108-127.

[23] Shu C.-W. (1988). Total-Variation-Diminishing time discretizations. *SIAM J. Sci. Stat. Comp.*, **9**, pp.1073-1084.

[24] Spitery R. J. and Ruuth S.J. (2002). A new class of optimal high-order strong-stability-preserving time discretization methods. *SIAM J. Numer. Anal.*, **40**, N 2, pp. 469-491.

[25] Takakura Y and Toro E.F. (2002). Arbitrarily accurate non-oscillatory schemes for a nonlinear conservation law. *CFD Journal*, **11**, N. 1, pp. 7-18.

[26] Titarev V.A. and Toro E.F. (2002). ADER: Arbitrary High Order Godunov Approach. *J. Sci. Comput.*, **17**, pp. 609-618.

[27] Titarev V.A. and Toro E.F. (2003) High order ADER schemes for the scalar advection-reaction-diffusion equations, *CFD Journal*, **12**, N. 1, pp. 1-6.

[28] Toro E.F. (1998). Primitive, conservative and adaptive schemes for hyperbolic conservation laws. In: *Numerical Methods for Wave Propagation*, pp 323-385. E F Toro and J F Clarke (editors). Kluwer Academic Publishers.

[29] Toro E.F. (1999). *Riemann Solvers and Numerical Methods for Fluid Dynamics.* Second Edition, Springer-Verlag.

[30] Toro E.F., Millington R.C. and Nejad L.A.M. (1998). Primitive upwind methods for hyperbolic partial differential equations. In *Sixteenth International Conference on Numerical Methods for Fluid Dynamics. C. H. Bruneau (Editor). Lecture Notes in Physics,* pp. 421-426, Springer-Verlag.

[31] Toro E.F., Millington R.C. and Nejad L.A.M. (2001). Towards very high order Godunov schemes. In: E. F. Toro (Editor). Godunov Methods. Theory and Applications, Edited Review, Kluwer/Plenum Academic Publishers, pp. 907-940, 2001.

[32] Toro E.F. and Titarev V.A. (2002). Solution of the Generalised Riemann Problem for Advection-Reaction Equations. *Proc. Roy. Soc. London*, 458(2018), pp. 271-281.

[33] Toro E.F and Titarev V.A. (2003). TVD Fluxes for the High-Order ADER Schemes, *to appear in Journal of Scientific Computing*, Preprint NI03011-NPA. Isaac Newton Institute for Mathematical Sciences, University of Cambridge, UK. - 2003. – 37 P.

[34] Toro E.F and Titarev V.A. (2003). ADER schemes for scalar hyperbolic conservation laws in three space dimensions. Preprint NI03063-NPA. Isaac Newton Institute for Mathematical Sciences, University of Cambridge, UK. - 2003. – 21 P., submitted.

[35] Toro E.F. (2003). Multi-stage predictor-corrector fluxes for hyperbolic equations. Preprint NI03037-NPA. Isaac Newton Institute for Mathematical Sciences, University of Cambridge, UK, *submitted to J. Comp. Phys.*

[36] Toro E.F., Spruce M. and Speares W. (1994). Restoration of the Contact Surface in the Harten-Lax-van Leer Riemann Solver. *Journal of Shock Waves*, **4**, pp. 25-34.

[37] Woodward P. and Colella P. (1984). The numerical simulation of two-dimensional fluid flow with strong shocks. *J. Comp. Phys.*, **54**, pp. 115-173.

[38] Zhang Y.-T., Shi J., Shu C.-W. and Zhou Y. (2003). Numerical viscosity and resolution of high-order weighted essentially nonoscillatory schemes for compressible flows with high Reynolds numbers. *Physical Review E*, **68**, article number 046709, pp.1-16.

[39] van Leer B. (1979). Towards the ultimate conservative difference Scheme V: a second order sequel to Godunov' method. *J. Comput. Phys.* **32**, pp. 101-136.